

Charge-transfer-driven enhanced room-temperature ferromagnetism in BiFeO₃/Ag nanocomposite

Tania Chatterjee,^{1,2} Shubhankar Mishra,³ Arnab Mukherjee,² Prabir Pal,⁴ Biswarup Satpati⁵ and Dipten Bhattacharya¹

¹Advanced Materials and Chemical Characterization Division, CSIR-Central Glass and Ceramic Research Institute, Kolkata 700032, India

²Functional Materials and Device Division, CSIR-Central Glass and Ceramic Research Institute, Kolkata 700032, India

³School of Materials Science and Nanotechnology, Jadavpur University, Kolkata 700032, India; Current address: Department of Physics, Indian Institute of Science, Bangalore 560012, India

⁴Material Characterization Division, CSIR-Central Glass and Ceramic Research Institute, Kolkata 700032, India

⁵Saha Institute of Nuclear Physics, a CI of Homi Bhabha National Institute, 1/AF Salt Lake, Kolkata 700064, India

E-mail: arnabm@cgcri.res.in

Abstract. We report observation of more than an order of magnitude jump in saturation magnetization in BiFeO₃/Ag nanocomposite at room temperature compared to what is observed in bare BiFeO₃ nanoparticles. Using transmission electron microscopy together with energy dispersive x-ray spectra (which maps the element concentration across the BiFeO₃/Ag interface) and x-ray photoelectron spectroscopy, we show that both the observed specific self-assembly pattern of BiFeO₃ and Ag nanoparticles and the charge transfer between Ag and O are responsible for such an enormous rise in room-temperature magnetization. The BiFeO₃/Ag nanocomposites, therefore, could prove to be extremely useful for a variety of applications including biomedical.

Keywords: BiFeO₃/Ag nanocomposite, charge transfer, ferromagnetism, magnetic force microscopy

1. Introduction

Decoration of malignant tumors with magnetic nanoparticles results in enhanced efficacy of the treatment by hyperthermia [1]. In this context, large room-temperature magnetization and soft ferromagnetism in a variety of bare or surface-functionalized oxide or alloy magnetic nanoparticles turns out to be especially useful. In recent time, nanoscale Fe₆₅Co₃₅ or Fe_{100-x}Co_x intermetallic alloys [2] (saturation magnetization $M_S \sim 240$ emu/g) or iron oxide nanoparticles [3, 4] ($M_S \sim 70-80$ emu/g) were used for such purposes. However, alloy systems are difficult to synthesize and often oxidize. Therefore, they are functionalized or capped by gold (Au) or silver (Ag) in the form of core-shell structure. This is, as well, necessary for making the structure biocompatible. In fact, attempts are being made [5, 6, 7, 8] to cap or functionalize magnetic nanoparticles by Au or Ag for different biomedical applications. Such structures, however, more often than not exhibit decrease in magnetization because of the capping or functionalization [9]. Motivated by these observations we attempted to examine whether capping by Ag could change the magnetization of nanoscale BiFeO₃ significantly and thus make them suitable for several applications including biomedical. This is all the more relevant for nanoscale BiFeO₃ since even bare nanoparticles of BiFeO₃ exhibit enhanced ferromagnetism at room temperature [10, 11, 12, 13, 14]. We report here that indeed decoration of multiferroic BiFeO₃ nanoparticles with Ag in the form of BiFeO₃/Ag nanocomposite results in an order of magnitude rise in saturation magnetization at room temperature than what is observed in bare BiFeO₃ nanoparticles. The charge transfer across the BiFeO₃/Ag interface and the specific pattern of self-assembly of the nanoparticles appear to be responsible for such an enormous enhancement in magnetization. This nanocomposite could be extremely useful for decoration of the malignant tumors necessary for efficacious hyperthermia. Because of magnetoelectric multiferroicity, the nanocomposite could be useful for ion channel gating action as well [15] where remote application of magnetic field can locally trigger onset of finite electric potential if BiFeO₃/Ag based multiferroic ion channel gates replace the faulty ones.

2. Experiments

The BiFeO₃/Ag nanocomposite was prepared by taking Bi(NO₃)₃, 5H₂O and Fe(NO₃)₃, 9H₂O in 1:1 molar ratio and directly dissolving them in 8M potassium nitrate solution. When the solution becomes homogeneous with dark brown color, 4 vol% of 5% hydrogen peroxide H₂O₂ (30% Merck) was added to the mixture and stirred well. The resultant solution was then transferred to a Teflon-lined autoclave for hydrothermal treatment for 30h at 180°C. The powder was collected by centrifugation and washed several times with de-ionized water and ethanol. The as-prepared BiFeO₃ particles were dispersed in 1:4 de-ionized water and ethanol mixture and sonicated until they were dissolved; 20 wt% silver nitrate (AgNO₃) was then added to the mixture. When the mixture became homogeneous, it was reduced by using NaBH₄ in 1:2 molar ratio. The solution immediately became dark brown and it was further stirred for 30 min. Finally, the powder was collected using a PVDF membrane filter of 0.22 μm pore size with the help of a vacuum filtration setup and washed by de-ionized water and ethanol mixture.

The nanocomposite, thus prepared, was characterized by powder x-ray diffraction. The particle morphology, pattern of self-assembly, and the concentration distribution

Charge-transfer-driven enhanced room-temperature ferromagnetism in BiFeO₃/Ag nanocomposite 3

of the elements (Bi, Fe, O, Ag) across different regions of the nanocomposite were investigated by using transmission electron microscopy (TEM) and energy dispersive x-ray spectra (EDX). The surface/interface electronic structure of Bi, Fe, O, and Ag was determined by x-ray photoelectron spectroscopy (XPS). The magnetization was measured by a Vibrating Sample Magnetometer (LakeShore Model 7407). The magnetic domain structure was imaged at room temperature by magnetic force microscopy (LT AFM/MFM System of Nanomagnetics Instruments Ltd., Ankara, Turkey).

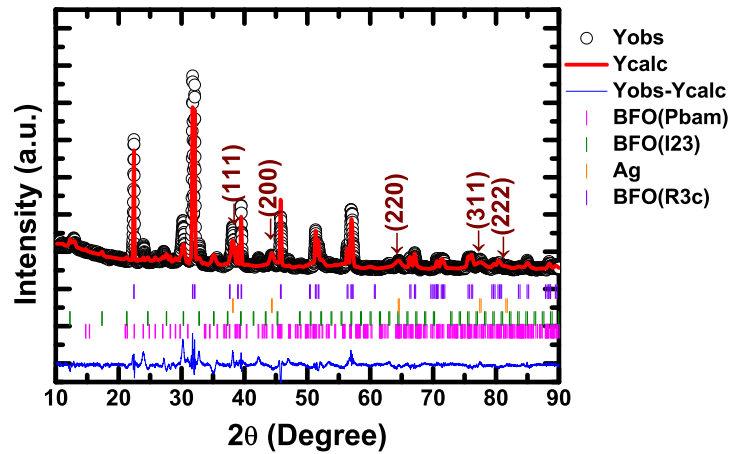


Figure 1. The room temperature powder x-ray diffraction (XRD) pattern and its refinement by FullProf. The peaks corresponding to Ag have been marked.

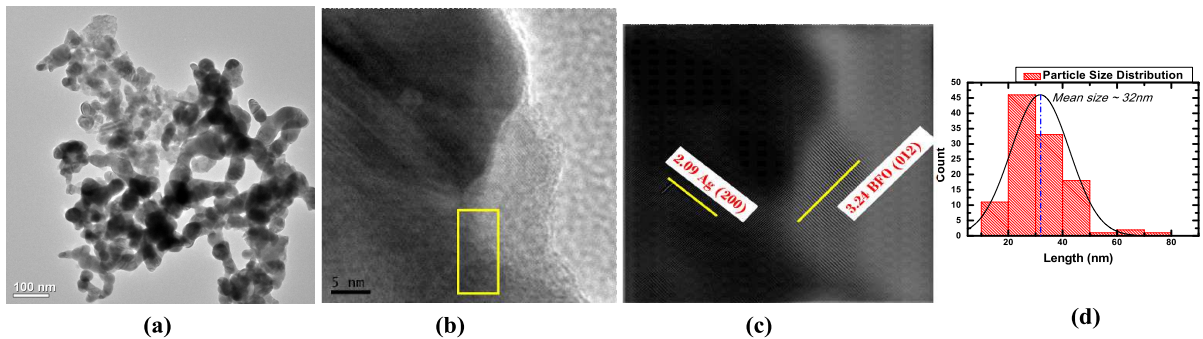


Figure 2. (a) Representative transmission electron microscopy (TEM) image of the BiFeO₃/Ag nanocomposite and (b), (c) high resolution TEM (HRTEM) image showing the presence of BiFeO₃ and Ag nanoparticles; image in (c) is obtained from the FFT and inverse FFT of the region shown in the box in (b); (d) the result of the TEM image analysis which shows that the average particle size is ~ 32 nm.

3. Results and Discussion

Figure 1 shows the room-temperature powder x-ray diffraction data of the BiFeO₃/Ag nanocomposite and their refinement by FullProf. The crystallographic structure turns out to be rhombohedral (*R3c* space group) with lattice parameters $a = b = 5.580$ Å and $c = 13.873$ Å. Peaks corresponding to Ag could also be observed. They are marked in Fig. 1. We used the JCPDS file 04-0783 for analyzing the peaks of Ag. Multiphase refinement yields the volume fraction of the respective phases - ~65% BiFeO₃ and ~20% Ag. Another sample with 2 vol% Ag has also been prepared. The Ag assumes cubic structure (space group *Fm3m*) with lattice parameter $a = 4.086$ Å. It is important to mention here that impurity Bi₂₅FeO₄₀ (space group *I23*) and Bi₂Fe₄O₉ (<5 vol%) (space group *Pbam*) phases were found to be present in the nanocomposite. However, we prepared a reference BiFeO₃ nanoscale sample which also contains these impurity phases. The x-ray diffraction data and their refinement for the reference sample are included in the supplemental materials document. We compared the magnetization data of these two nanocomposites for highlighting the influence of Ag decoration. Comparison with the data of bare BiFeO₃ nanoparticles does not indicate formation of BiFeO₃/Ag solid solution. This is corroborated by the scanning transmission electron microscopy (STEM) and energy dispersive x-ray (EDX) mapping data (discussed later) where the concentration of Ag has been mapped across the nanoparticles. The high resolution TEM (HRTEM) data too point out that nanoparticles of Ag and BiFeO₃ exists side-by-side; Ag does not affect the lattice of BiFeO₃. Interface interaction appears to be more important in the present case. The structural details such as the space group, lattice parameters, ion positions, as well as the fit statistics for both the samples (one which contains Ag and another which does not contain Ag) are available in the supplementary materials document (Table S-I).

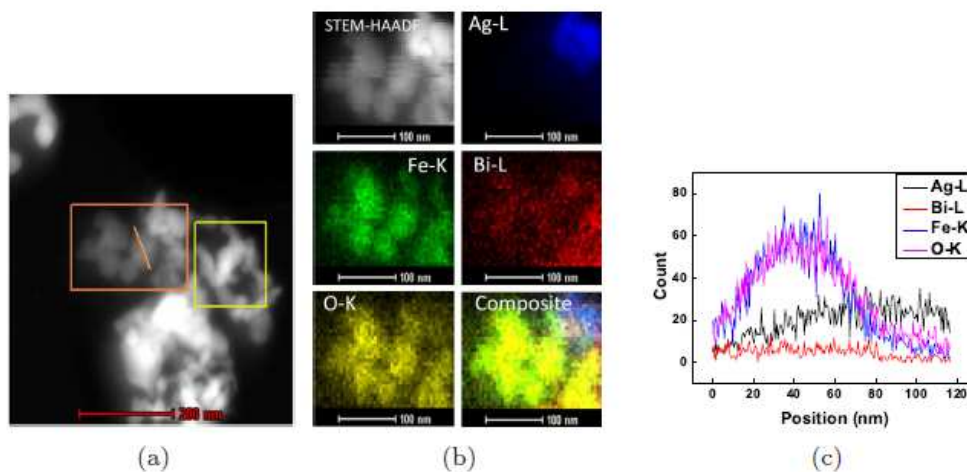


Figure 3. (a) Representative STEM-HAADF image of the BiFeO₃/Ag nanocomposite; (b) mapping of the distribution of element (Bi, Fe, O, and Ag) concentration across the nanocomposite obtained from the energy dispersive x-ray spectra recorded; (c) the mapping of the quantitative data on element concentration across the line shown in image (a).

The particle morphology, self-assembly pattern, and the charge transfer across the

BiFeO₃ and Ag nanoparticle interface were investigated in detail by TEM, EDX, and XPS. Figure 2 shows the representative bright-field TEM images of the nanocomposite across different length scales. The pattern of self-assembly and the particle size could be observed and determined from these images. The average size of the particles is ~ 32 nm. It corroborates the result obtained (~ 35 nm) from the calculation of crystallite size using the line broadening of the x-ray diffraction data (supplementary materials document). It appears that a chain-like self-assembled structure has formed with finer Ag nanoparticles (average size ~ 5 nm) surrounding the BiFeO₃ ones. The representative TEM image of the nanoscale BiFeO₃ reference sample (average particle size ~ 32 nm) is included in the supplementary materials document. We recorded the high resolution TEM images across the BiFeO₃ and Ag nanoparticle interfaces. The images were fast Fourier transformed (FFT) and then inverted (inverse FFT) to generate clearer views of the lattice fringes. The corresponding ‘d’ values were determined. It appears that (012) plane of BiFeO₃ and (200) plane of Ag nanoparticles are oriented perpendicular to the electron beam. Additional images showing the orientation of the (104) and (111) planes of, respectively, BiFeO₃ and Ag are included in the supplementary materials document. The scanning transmission electron microscopy (STEM) and the high-angle annular dark field (HAADF) images were also recorded at different regions of the nanocomposite (Fig. 3). The EDX mapping of the elements Bi, Fe, O, and Ag across those regions confirms the distribution pattern of the BiFeO₃ and Ag nanoparticles. In order to obtain a clearer view, the line scans of the element concentration were recorded across the interfaces between the BiFeO₃ and Ag nanoparticles at different regions of the nanocomposite (Fig. 3). Additional images and line scan data are available in the supplementary materials document. Combining the TEM, HRTEM, STEM images and the mapping of the concentration of the elements across the interfaces between BiFeO₃ and Ag nanoparticles by line scans it is possible to clearly notice how the nanoparticles are distributed or, in other words, the specific self-assembly patterns of the BiFeO₃ and Ag nanoparticles. Such a pattern of self-assembly appears to have maximized the interface area which, in turn, yields such enormous rise in saturation magnetization.

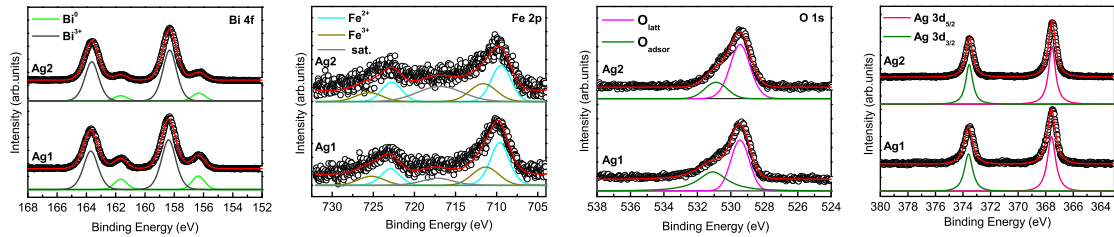


Figure 4. The x-ray photoelectron spectra for (a) Bi, (b) Fe, (c) O, and (d) Ag and their fitting.

The charge states of the ions have been examined by x-ray photoelectron spectroscopy (XPS). In Fig. 4, we show the spectra corresponding to the Bi, Fe, O, and Ag ions. The peaks have been fitted by using appropriate model following the background subtraction and tabulated in the Table-1. The peaks corresponding to Bi³⁺ state are located at ~ 158.3 and ~ 163.7 eV, respectively. It indicates that no doping or substitution has taken place at the Bi-site. Small amount of metallic

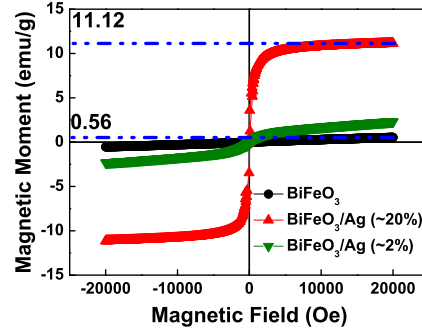


Figure 5. The room temperature M - H hysteresis loops for the BiFeO₃ nanoparticles (reference sample) and the BiFeO₃/Ag nanocomposites containing ~ 2 and ~ 20 vol% Ag.

Bi⁰ phase could be observed with corresponding peaks at ~ 156.3 and ~ 161.6 eV. The fitted Fe 2p spectra show the presence of characteristic doublet peaks of Fe(II)-O species at ~ 709.5 and ~ 723.0 eV for Fe 2p_{3/2} and Fe 2p_{1/2}, respectively. The corresponding doublet peaks of Fe(III)-O species are present at ~ 711.6 and ~ 725.5 eV, respectively. The O 1s spectra contain characteristic features at ~ 529.5 and ~ 530.9 eV which correspond to the lattice oxygen and loss of oxygen, respectively. In the Ag 3d spectra, the characteristic doublet peaks could be observed at ~ 367.5 and ~ 373.6 eV. Comparison with the XPS spectra for pure BiFeO₃ and Ag shows the presence of a shift of ~ 0.7 eV in the spectra of Ag and lattice oxygen of BiFeO₃. It points out orbital overlap and charge transfer between Ag and O states in the BiFeO₃/Ag nanocomposite. Contrary to the observations made in other cases, in the present case, electron transfer appears to have taken place from O to Ag creating holes in the O p states. The O 1s core level spectra of BiFeO₃/Ag nanocomposite clearly show an increase in high binding energy shoulder compared to that of BiFeO₃ sample, which is generally attributed to surface oxygen vacancies and/or adsorbed contaminant.

Figure 5 shows the room temperature magnetization (M) versus applied magnetic field (H) magnetic hysteresis loops for the reference BiFeO₃ nanoparticles and BiFeO₃/Ag nanocomposites containing ~ 2 and ~ 20 vol% Ag. Clearly, more than an order of magnitude jump in saturation magnetization (M_S) could be observed [from ~ 0.56 emu/g ($\sim 0.03 \mu_B$ /formula unit) to ~ 11.12 emu/g ($\sim 0.6 \mu_B$ /formula unit)] in the nanocomposite with ~ 20 vol% Ag. The coercivity H_C , of course, turns out to be quite small (~ 60 Oe). Presence of Ag indeed gives rise to enhancement of ferromagnetism. We also measured the zero-field-cooled (ZFC) and field-cooled (FC) magnetization versus temperature patterns across 300-700 K. The result is included in the supplementary materials document. The transition temperature T_N turns out to be ~ 550 K. We further employed magnetic force microscopy (MFM) to observe the influence of large saturation magnetization on the phase contrast as well as on the magnetic domain structure. The nanocomposite (with ~ 20 vol% Ag) particles were dispersed in ethanol and deposited onto a glass substrate. The dried substrate was used for recording the MFM scan. Figure 6 shows the MFM topography and the phase-contrast images. They were processed by Gwyddion software. The line scans recorded across different regions of the phase-contrast image (Fig. 6b) reveals

Table 1. The XPS peaks for bare BiFeO₃, Ag, and BiFeO₃/Ag nanocomposite.

Ion	Ionic state	BiFeO ₃ /Ag	Bare BiFeO ₃	shift
Bi4f	Bi ^o	156.3	156.8	-0.5
	Bi ^o	161.6	162.1	-0.5
	Bi ³⁺	158.3	158.8	-0.5
	Bi ³⁺	163.7	164.1	-0.5
Fe2p	Fe ²⁺	709.5	710.7	-1.2
	Fe ²⁺	723.0	724.2	-1.2
	Fe ³⁺	711.6	711.4	0.2
	Fe ³⁺	725.5	725.3	0.2
	Sat	716.9	717.6	
O1s	Lattice O	529.5	528.8	0.7
	O vacancy	530.9	529.7	1.2
	Surface O		531.0	
Ag3d		Ag	Bare Nano	
	3d 5/2	367.5	368.2	-0.7
	3d 3/2	373.6	374.2	-0.7

the size of the magnetic domains in different regions of the nanocomposite cluster. The lines are shown in the phase contrast image. The corresponding plot shows the average size of the domains (Fig. 6e). It turns out to be 1.0-1.5 μm . Therefore, across the particle clusters, the magnetic domains form by encompassing large number of individual particles. This has been observed by others as well [16]. We compare the phase-contrast data observed in this case with those obtained for the reference BiFeO₃ nanoparticle cluster and the standard magnetic thin film (surface of magnetic hard disk) (Fig. 6f) - black, red, and blue lines (Fig. 6f), respectively, represent the phase-contrast line profiles for the reference BiFeO₃ cluster, magnetic hard disk, and the BiFeO₃/Ag (~ 20 vol%) nanocomposite cluster. The corresponding phase-contrast MFM images are shown in Figs. 6(c) and (d), respectively. Clearly, the phase contrast is enormous in the case of the BiFeO₃/Ag nanocomposite. Since, $\Delta\phi \propto K_p \cdot \partial F_z / \partial z$ [17, 18], large force gradient ($\partial F_z / \partial z$) resulting from large stray field gradient leads to large $\Delta\phi$. It is important to mention here that the same cantilever (Co-alloy coated Si cantilever-tip, coercivity ~ 300 Oe) has been used to map the MFM images for all the samples - hard disk surface, BiFeO₃ nanoparticles, and BiFeO₃/Ag nanocomposite. Therefore, the constant factor K_p remains invariant in all these cases. The plot in Fig. 6f shows that the $\Delta\phi$ in the nanocomposite is even higher than that in the hard disk. Therefore, the signature of large magnetization could be observed in MFM images as well. The crosstalk between topography and phase-contrast images in MFM, of course, often poses difficulty in imaging the magnetic domains clearly. However, since the magnetization is large in the present case (resulting in large stray field gradient and hence large phase contrast $\Delta\phi$) and dual pass technique with large cantilever lift height (~ 120 - 150 nm) has been used, the influence of topography on the phase-contrast images is minimal. The utility of dual pass technique and large cantilever lift height in eliminating the influence of topography on phase-contrast MFM images has

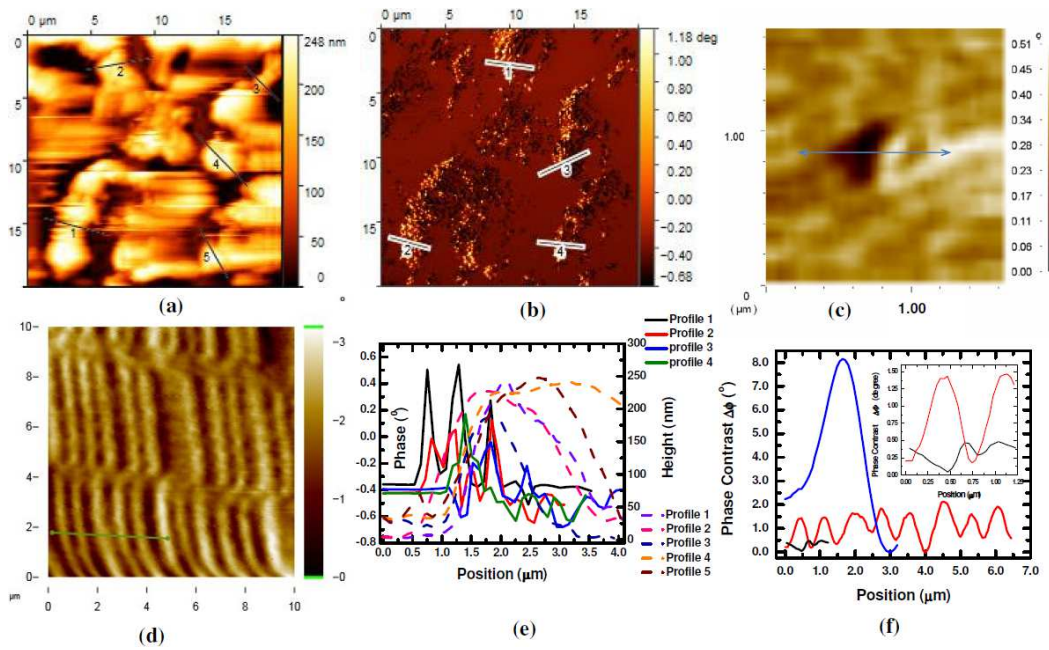


Figure 6. Representative magnetic force microscopy (MFM) (a) topography and (b) phase-contrast images of the BiFeO₃/Ag nanoclusters containing ~20 vol% Ag, (c) and (d) are the representative phase-contrast MFM images of the BiFeO₃ nanoparticle cluster and hard-disk surface commonly used in MFM as a standard sample; (e) line scan mapping of the topography and phase-contrast MFM images [corresponding lines are shown, respectively, in (a) and (b)] which indicates the size of the nanoparticle clusters and the magnetic domain size; the solid lines represent the magnetic domain size (left axis) while the dashed lines represent the size of the nanoparticle clusters (right axis); (f) line scan data with normalized phase contrast ($\Delta\phi$) for different samples - BiFeO₃/Ag nanocomposite (blue line), pure BiFeO₃ (black line), and the hard disk (red line); inset zooms in on the data for BiFeO₃ nanoparticles (black line) and hard disk (red line).

been highlighted by others as well [19]. The line scans, taken on the topography image (Fig. 6a), reveals the difference between the nanoparticle cluster size and the size of the magnetic domains (Fig. 6e). This difference highlights the negligible influence of topography on the phase-contrast MFM image. In fact, complete reversal of the magnetic domains could also be observed [20] even in bare BiFeO₃ nanoparticles upon reversal of applied magnetic field (+20 and -20 kOe). Additional MFM images of magnetic domain reversal due to reversal of applied magnetic field, observed in bare BiFeO₃ nanoparticles, are available in the supplementary materials document.

Neither bare BiFeO₃ nanoparticles of average size ~30 nm nor bare Ag⁰ nanoparticles exhibit such a large magnetization. Though the ferromagnetism indeed depends on particle size in nanoscale BiFeO₃ [21], we compared here magnetic properties of two samples of comparable average particle size (~30 nm) to rule out the influence of particle size. A cluster of Ag nanoparticles, on the contrary, is theoretically predicted [22] to be giving rise to ferromagnetism because of charge transfer driven by symmetry of the cluster. Charge transfer between Ag 4d and O 2p states was also

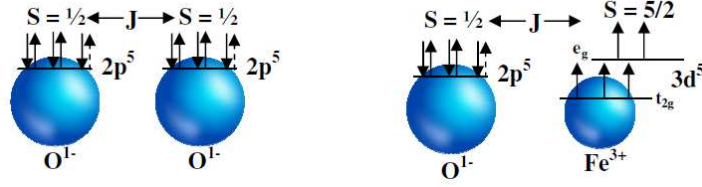


Figure 7. The schematic of the possible exchange coupling interactions across O⁻-O⁻ and O⁻-Fe³⁺ channels which indicate the additional magnetic interactions resulting from charge transfer between O and Ag.

shown to be resulting in ferromagnetism if Ag films are exposed to oxygen [23]. In MoS₂/Ag nanocomposite, it was earlier observed [24] that the holes in Ag 4d level and formation of Ag-S bonds (resulting from charge transfer between Ag and S) could induce ferromagnetism and metal-insulator transition. In the present case, the XPS data suggest that the charge transfer has taken place from O to Ag and thus creating holes in the O 2p states. As a result, it appears that alongside Ag 5s²4d¹⁰ states, O 2p⁵ states ($S = \frac{1}{2}$) could possibly emerge here in this nanocomposite from O 2p⁶ states in pure BiFeO₃. The charge state shift, observed in Ag, has also been noticed in nanoscale Ag by others [25]. In such a situation, in addition to the existing magnetic exchange interaction channels, exchange interactions could take place across the O⁻-O⁻ and Fe³⁺-O⁻ channels as well (Fig. 7). Therefore, p-state ferromagnetism seems to be assuming relevance in this case. Ferromagnetism due to p electrons in C around the vacancies in Si and C sites or due to trapping of holes in O sites nearest to the vacancies in Mg in MgO nanocrystals were earlier shown [26, 27] in SiC and MgO. Oxidization of oxygen and consequent trapping of holes or even molecular O₂ formation was earlier observed [28] in Na_{0.6}(Li_{0.2}Mn_{0.8})O₂ system during charge-discharging cycles of a battery where Na_{0.6}(Li_{0.2}Mn_{0.8})O₂ was used as the cathode. Of course, the oxidation states of Ag and O here and the origin of additional ferromagnetism, as a result, need to be probed in greater detail. This will be attempted in a future work. It is important to mention here that, in nanoscale magnetic oxides, the magnetization is generally expected to be influenced by uncompensated spins arising out of surface defects. The surface defects of Ag-free nanosized BiFeO₃ particles were earlier studied by XPS [29]. But, the magnetization data for the reference (i.e., Ag-free) BiFeO₃ sample clearly show that the BiFeO₃/Ag nanocomposite, comprising of nanoparticles of comparable size (~30-32 nm), exhibits more than an order of magnitude jump in magnetization. Therefore, the distinct influence of Ag and consequent charge transfer is discernible in the case of the nanocomposite. Further we point out that even though the Bi₂₅FeO₄₀ and Bi₂Fe₄O₉ phases are present in the nanocomposite, they do not contribute much to the room temperature ferromagnetism since the magnetic transition temperature (T_N) of these compounds are around 272 K [30] and 250 K, respectively. Moreover, these impurity phases are found to be present in the reference BiFeO₃ sample (which is used here for comparing the magnetization) as well.

4. Summary

In summary, we report observation of more than an order of magnitude jump in room-temperature saturation magnetization in BiFeO₃/Ag nanocomposite. This could be

p-state ferromagnetism resulting from charge transfer between Ag and O. Both the saturation magnetization and the magnetic phase contrast (observed in MFM imaging) turn out to be quite enormous. Soft ferromagnetism with such a large saturation magnetization at room temperature could be extremely useful for various applications including biomedical, especially, decoration of malignant tumors necessary for efficacious treatment.

Acknowledgements

Two of the authors (TC, SM) acknowledge DST-INSPIRE fellowship, Govt of India, during this work. Another author (A.M.) acknowledges support from Science and Engineering Research Board (SERB), Government of India (grant no. CRG/2021/002132).

Data availability statement

The data of this paper are available in the main paper as well as in the supplementary materials document (to be provided on request).

References

- [1] See, for example, Giustini A J, Petryk A A, Cassim S M, Tate J A, Baker I and Hoopes P J 2010 Magnetic nanoparticle hyperthermia in cancer treatment *Nano Life* **1** 17 (doi: 10.1142/S1793984410000067)
- [2] Jesus F S, Bolarin-Miro A M, Escobedo C A C, Torres-Villasenor G and Vera-Serna P Structural analysis and magnetic properties of FeCo alloys obtained by mechanical alloying 2016 *J. Metal.* **2016** 8347063
- [3] Woo K, Hong J, Choi S, Lee H-W, Ahn J-P, Kim C S and S.W. Lee S W 2004 Easy synthesis and magnetic properties of iron oxide nanoparticles *Chem. Mater.* **16** 2814
- [4] Laurent S, Forge D, Port M, Roch A, Robic C, Elst L V and Muller R N 2008 Magnetic iron oxide nanoparticles: synthesis, stabilization, vectorization, physicochemical characterizations and biological applications *Chem. Rev.* **108** 2064
- [5] Dabagh S, Asadi Haris S, Isfahani B K and Ertas Y N 2023 Silver-decorated and silica-capped magnetite nanoparticles with effective antibacterial activity and reusability *ACS Applied Biomater.* **6** 2266-2276
- [6] Brollo M E F, Lopez-Ruiz R, Muraca D, Figueroa S J A, Pirota K R and Knobel M 2014 Compact Ag@Fe₃O₄ core-shell nanoparticles by means of single-step thermal decomposition reaction *Sci. Rep.* **4** 6839
- [7] Felix L L, Sanz B, Sebastian V, Torres T E, Sousa M H, Coaquira J A H, Ibarra M R and Goya G F 2019 Gold-decorated magnetic nanoparticles design for hyperthermia applications and as a potential platform for their surface functionalization *Sci. Rep.* **9** 4185
- [8] Anik M I, Hossain M H, Hossain I, Mahfuz A. M U. B., Rahman M T and Ahmed I 2021 Recent progress of magnetic nanoparticles in biomedical applications: a review *Nano Select* **2** 1146-1186
- [9] Takahashi M, Mohan P, Nakade A, Higashimine K, Mott D, Hamada T, Matsumura K, Taguchi T and Maenosono S 2015 Ag/FeCo/Ag core/shell/shell magnetic nanoparticles with plasmonic imaging capability *Langmuir* **31**, 2228
- [10] Park T J, Papaefthymiou G C, Viascas A J, Moodenbough A R and Wong S S 2007 Size-dependent magnetic properties of single-crystalline multiferroic BiFeO₃ nanoparticles *Nano Lett.* **7** 766-772
- [11] Maumder R, Devi P S, Bhattacharya D, Choudhury P, Sen A and Raja M 2007 Ferromagnetism in nanoscale BiFeO₃ *Appl. Phys. Lett.* **91** 062510
- [12] Carranza-Celis D, Cardona-Rodriguez A, Narvaez J, Moscoso-Londono O, Muraca D, Knobel M, Ornelas-Soto N, Reiber A and Ramirez J G 2019 Control of multiferroic properties in BiFeO₃ nanoparticles *Sci. Rep.* **9** 3182
- [13] Ramos E, Cardona-Rodriguez A, Carranza-Celis D, Gonzalez-Hernandez R, Muraca

- D and Ramirez J G Strain-controlled ferromagnetism in BiFeO₃ nanoparticles *J. Phys. Condens. Matter* **32** 185703
- [14] Cardona-Rodriguez A, Rodriguez E R, Carranza-Celis D, Vergara-Duran N, da Cruz A S E, Moscoso-Londono O, Beron F, Knobel M, Reiber A, Muraca D and Ramirez J G 2022 Resolving magnetic contributions in BiFeO₃ nanoparticles using First Order reversal curves *J Magn. Magn. Mater.* **556** 169409
- [15] See, for example, Kargol A, Malkinski L and Caruntu G 2012 Biomedical applications of multiferroic nanoparticles in *Advanced Magnetic Materials*, edited by L. Malkinski (InTech, Rijeka), Chap. 4.
- [16] See, for example, Puentes V F, Gorostiza P, Aruguete D M, Bastus N G and Alivisatos A P 2004 Collective behaviour in two-dimensional cobalt nanoparticle assemblies observed by magnetic force microscopy *Nat. Mater.* **3** 263
- [17] Gomez R D, Pak A O, Anderson A J, Burke E R, Leyendecker A J and Mayergoyz I D 1998 Quantification of magnetic force microscopy images using combined electrostatic and magnetostatic imaging *J. Appl. Phys.* **83** 6226
- [18] Kazakova O, Puttock R, Barton C, Corte-Lion H, Jaafar M, Neu V and Asenjo A 2019 Frontiers of magnetic force microscopy *J. Appl. Phys.* **125** 060901
- [19] See, for example, Freire O, Advances in magnetic force microscopy (PhD thesis, Materials Science Institute of Madrid, 2014) (<https://core.ac.uk/download/pdf/36161652.pdf>); Maldovan A and Dinescu M 2022 Single-pass magnetic force microscopy technique, with topography feedback based on scanning polarization force microscopy *Appl. Surf. Sci.* **597** 153747; Parker A C, Maryon O O, Kaffash M T, Jungfleisch M B and Davis P H 2022 Optimizing magnetic force microscopy resolution and sensitivity to visualize nanoscale magnetic domains *J. Visualized Expt.* **185** e64180
- [20] See, for example, Goswami S, Sahoo A, Bhattacharya D, Karci O and Mohanty P K 2020 Large structure-dependent room temperature exchange bias in self-assembled BiFeO₃ nanoparticles 2020 *APL Mater.* **8** 081101
- [21] See, for example, Hasan M, Islam M F, Mahub R, Hossain M S and Hakim M A 2016 A soft chemical route to the synthesis of BiFeO₃ nanoparticles with enhanced magnetization *Mater. Res. Bull.* **73** 179
- [22] Pereiro M, Baldomir D and Arias J E 2007 Unexpected magnetism of small silver clusters *Phys. Rev. A* **75** 063204
- [23] Marengo A J, Pedersen D B and Trudel S 2017 On the origin of ferromagnetic signature in silver nanoparticles and thin films *J. Mater. Chem. C* **5** 4899; see also, e.g., Coey J M D, Wongsaprom K, Alaria J and Venkatesan M 2008 Charge-transfer ferromagnetism in oxide nanoparticles *J. Phys.D: Appl. Phys.* **41** 134012
- [24] Bag S, Bhattacharya S, Dinda D, Jyothirmai M V, Thapa R and Saha S K 2018 Induced ferromagnetism and metal-insulator transition due to a charge transfer effect in silver nanoparticle decorated MoS₂ *Phys. Rev. B* **98** 014109
- [25] Huang Z, Jiang H, Liu P, Sun J, Guo D, Shan J and Gu N 2015 Continuous synthesis of size-tunable silver nanoparticles by a green electrolysis method and multi-electrode design for high yield *J. Mater. Chem. A* **3** 1925-1929
- [26] Wang Y, Liu Y, Wang G, Anwand W, Jenkins C A, Arenholz E, Munnik F, Gordan O D, Salvan G, Zahn D R T, Chen X, Gemming S, Helm M and Zhou S 2015 Carbon p electron ferromagnetism in silicon carbide *Sci. Rep.* **5** 8999
- [27] Choudhury B, Saikia U, Sahariah M B, Choudhury A 2020 Vacancy induced p-orbital ferromagnetism in MgO nanocrystallite *J. Alloys Compds.* **819** 153060
- [28] House R A, Rees G J, McColl K, Marie J.J., Fernandez M G, Nag A, Zhou K-J, Cassidy S, Morgan B J, Islam M S and Bruce P G 2023 Delocalized electron holes on oxygen in a battery cathode *Nat. Energy* **8** 351-360
- [29] Chatterjee T, Mukherjee A, Pal P, Kaushik S D, Siruguri V, Mandal S, Hazra S, Bhattacharjee S, Ghosh C K and Bhattacharya D 2022 Nonmonotonic magnetic field dependence of remnant ferroelectric polarization in reduced graphene oxide-BiFeO₃ nanocomposite *Phys. Stat. Solidi RRL* **16** 2200077
- [30] Jebari H, Tahiri N, Boujnah M, El Bounagui O, Taibi M and Ez-Zahraouy H 2021 Theoretical investigation of electronic, magnetic and magnetocaloric properties of Bi₂₅FeO₄₀ compound *Phase Trans.* **94** 147-158